JSTARS-2022-00399

Empirical Bayesian Estimation of the Interferometric SAR Coherence Magnitude

Nico Adam, http://orcid.org/0000-0002-6053-0105

***Abstract*— SAR interferometry has developed rapidly in recent years and now allows measurements of subtle deformation of the Earth's surface with millimeter accuracy. All state-of-the-art processing methods require a precise coherence estimate. However, this estimate is a random variable and biased toward higher values. Up to now, little is published on the Bayesian estimation of the degree of coherence. The objective of the paper is to develop empirical Bayesian estimators and to assess their characteristics by simulations. Bayesian estimation is understood as a regularization of the maximum likelihood estimation. The more information is used and the stricter the general prior, the more accurate the estimate will be. Three levels of prior information are developed: (1) an uninformative prior and (2) an informative prior which can be implemented as (2a) less strict prior and (2b) strict prior. The informative priors are described by a single parameter only i.e. the maximum underlaying coherence. The paper reports on the bias, the standard deviation and the root mean square error (RMSE) of the developed estimators. It was found that all empirical Bayes estimators improve the coherence estimation from small samples and for small underlaying coherences compared to the conventional sample estimator. E.g. a zero underlaying coherence is estimated by the expected a posteriori estimator without additional information with a 33.3% reduced bias using three samples only. Assuming the maximum underlaying coherence is 0.6, the bias is reduced by 51.3% for the strict prior and by 36.6% for the less strict prior. In addition, it was found that the methods work very well even for the extremely small sample size of only 2 values.**

***Index Terms*—Bayesian inference, Coherence magnitude, Degree of coherence, Distributed Scatterers in SqueeSAR or CESAR or phase linking, Empirical Bayes method, Expected a posteriori estimation, Interferometric SAR (InSAR), Maximum a posteriori estimation, Median a posteriori estimation**

I. INTRODUCTION

Spaceborne SAR interferometry (InSAR) is a well-established monitoring technique for the generation of digital elevation models (DEMs) and the displacement of the Earth's surface. In this field of work, the coherence magnitude was originally established as a quality measure in form of quicklooks and layer to support phase unwrapping [1]. Practically, it is a proxy for the signal to noise ratio (SNR) as pointed out by Zebker and Villasenor [2] as well as Just and Bamler [3]. In recent years, the importance of the coherence magnitude has increased significantly. All state-of-the-art processing methods for the observation of subtle deformation of the Earth with millimeter accuracy require precise coherence estimates [4], [5], [6] and [7]. Cao *et al.* [8] provide an overview on the mathematical framework showing the degree of coherence is the essential weighting in all estimation methods. In operational systems, the sample coherence magnitude is typically implemented. However, the estimate itself is a random variable and biased toward higher values. The respective statistic has been provided by Touzi and Lopes [9]. Touzi *et al.* also have proposed two methods in order to mitigate the bias [10]. The first method inverts the functional relation between the first moment of the sample coherence magnitude estimate and the true coherence. For the applicability of this method, the authors state that the number of samples must be sufficiently large. As an alternative method, the authors briefly mention that the maximum a posteriori estimation based on a uniform prior may be adapted. Zebker and Chen [11] have developed a method to correct the bias fitting a polynomial to correlation estimates of simulated data as a function of true correlation and the number of looks in the estimate. Another work on bias removal for coherence magnitude estimation has been published by Abdelfattah and Nicolas [12]. In this work, the coherence is computed from the logarithm of the sample coherence named second kind statistic. More recently, Jiang *et al.* [13] demonstrated the mitigation of the sample coherence bias with only several samples based on Double Bootstrapping. Up to now, little is published on the Bayesian principle in the context of coherence estimation although it is well established in other areas and the advantages are widely recognized. Nowadays, Bayesian estimation is understood as a regularization of the maximum likelihood estimation. This is the reason, an improved estimation compared to the maximum likelihood estimator is expected. The specific objectives of the paper are summarized as follows.

i. The principle of the empirical Bayes approach is explained.
ii. Three basic Bayesian estimator principles are compared, namely the maximum a posteriori (MAP), the expected a posteriori (EAP) and the median a posteriori (MEDAP) estimators.
iii. Estimators with uninformative and informative prior are developed.
iv. For the informative prior, two typical InSAR scenarios are being considered i.e. a strict prior and a less strict prior.
v. The characteristics of the estimators are evaluated numerically by simulations and presented.

Manuscript received April 5, 2022; (Corresponding author: Nico Adam.)
Nico Adam is with the German Aerospace Center (DLR), Oberpfaffenhofen, Germany (e-mail: nico.adam@dlr.de).
Digital Object Identifier …

vi. The results are generalized for use in operational systems.

This paper is organized as follows. Section II describes the methods. Respective simulation results are provided for the maximum a posteriori (MAP), the expected a posteriori (EAP), the median a posteriori (MEDAP), the strict (EAPSP) and the less strict (EAPLSP) general prior EAP estimators in section III. In section IV, the characteristics of these methods are discussed and the results are generalized for use in operational systems. Finally, section V presents the conclusions.

II. Methods

A complex SAR scene pixel $x_{k,i} = a_{k,i} exp(j\,\delta_{k,i})$ is a sum of random contributions from many individual scatterers within the resolution cell. The variable $x_{k,i}$ denotes the single look complex SAR scene with index $k = 1$ for the primary and $k = 2$ for the secondary scene. i is the pixel index within the scene corresponding to the location of the pixel. In all InSAR data, the location of a pixel is two dimensional (i.e. range and azimuth respectively fast and slow time). However, it has no relevance for the estimation and a single index i within the homogenous region is sufficient. According to Goodman [14] and Just and Bamler [3], radar scenes are modelled by a complex, circular, stationary Gaussian (CCG) process assuming (i) the amplitude and phase of all elementary scatterers are statistically independent and (ii) all phases are equally likely in the interval [-π,π). This means the real $Re(x_{k,i})$ and imaginary $Im(x_{k,i})$ parts are independent Gaussian distributed random variables, $E\{Re(x_{k,i})\} = 0$ and $E\{Im(x_{k,i})\} = 0$ with $x_{k,i} = Re(x_{k,i}) + j\,Im(x_{k,i})$, the standard deviation of the real part σ_{re} is the same as of the imaginary component σ_{im} i.e. $\sigma_{re} = \sigma_{im} = \sigma$, the scattering surface is rough with respect to the wavelength and a homogenous area is detected providing a spatially homogenous backscatter coefficient and a stationary phase signal (i.e. residual topography, deformation and atmospheric phase screen are compensated).

For an interferogram, a 2 x 2 covariance matrix describes the relation of the respective CCG processes. This matrix contains the expected intensities on the diagonal and the covariances on the off-diagonal. The covariance is defined for the random variables X_1 and X_2 i.e. for the primary and the secondary signal by

$$Cov(X_1, X_2) = E\{X_1\,X_2\} - E\{X_1\}\,E\{X_2\}. \quad (1)$$

$E\{.\}$ is the expected value operator i.e. the ensemble average. The linear correlation coefficient ρ_{X_1,X_2} is defined by the normalization

$$\rho_{X_1,X_2} = \frac{Cov(X_1,X_2)}{\sqrt{Var\{X_1\}}\sqrt{Var\{X_2\}}}. \quad (2)$$

For a CCG process, (1) simplifies with $E\{X_1\} = 0$ and $E\{X_2\} = 0$ and the complex coherence is

$$\gamma = \frac{E\{X_1 X_2^*\}}{\sqrt{E\{|X_1|^2\}}\sqrt{E\{|X_2|^2\}}}. \quad (3)$$

The principle of ergodicity allows using the spatial mean instead of the ensemble average and gives the sample estimator of the coherence coefficient $\hat{\gamma}_s$ based on N independent and identically distributed (i.i.d.) samples.

$$\hat{\gamma}_s\, e^{j\,\hat{\varphi}_s} = \frac{\sum_{i=1}^{N} x_{1,i}\, x_{2,i}^*}{\sqrt{\sum_{i=1}^{N}|x_{1,i}|^2}\sqrt{\sum_{i=1}^{N}|x_{2,i}|^2}} \quad (4)$$

The Bayesian analysis is based on the posterior distribution of the processes underlaying true coherence γ which is constructed by Bayes' theorem from the data samples D [15].

$$p(\gamma \mid D) = \frac{p(D \mid \gamma)\, p(\gamma)}{\int_{\gamma=-1}^{1} p(D \mid \gamma)\, p(\gamma)\, d\gamma} \quad (5)$$

In SAR interferometry, the data samples are available in pairs from the two single look complex (SLC) scenes $D = \{x_{1,i}, x_{2,i} | i = 1, .., N\}$. That is, D denotes all pairs of samples of a homogeneous region. The likelihood function $p(D \mid \gamma)$ is proportional to the probability of receiving the data D if the coherence γ was the basis. $p(\gamma)$ is the prior and corresponds to a hypothesis on the coherence γ. In the equation above, the denominator is named evidence. It is the normalization which makes the posterior a proper probability density distribution. It is apparent that the posterior coherence γ is a random variable described by the posterior $p(\gamma \mid D)$ in contrast to the γ in the likelihood $p(D \mid \gamma)$. This is the reason, the coherence is estimated to be the mode for the maximum a posteriori estimator

$$\hat{\gamma}_{MAP} = \arg\max_{\gamma} p(\gamma \mid D) \quad (6)$$

or the expected value of the posterior distribution for the expected a posteriori estimator

$$\hat{\gamma}_{EAP} = E\{p(\gamma \mid D)\} \quad (7)$$

or the median value of the posterior distribution for the median a posteriori estimator

$$\hat{\gamma}_{MEDAP} = Median\{p(\gamma \mid D)\}. \quad (8)$$

The mode, mean and median of the posterior distribution $p(\gamma \mid D)$ make a difference because of the skewness of this distribution. Assuming independent and identically distributed random variables in each SAR scene $x_{1,i}$ and $x_{2,i}$, the likelihood function $p(D \mid \gamma)$ is the product of the N individually joint probability density functions (PDFs) $p(x_{1,i}, x_{2,i} \mid \gamma, \varphi)$.

$$p(D \mid \gamma) = \prod_{i=1}^{N} p(x_{1,i}, x_{2,i} \mid \gamma, \varphi) \quad (9)$$

The individually joint PDFs were published by Touzi and Lopes [9] as a function of the sample pair's amplitudes $a_{k,i}$ and phase difference $\delta_i = \delta_{2,i} - \delta_{1,i}$ given the underlaying coherence γ and interferometric phase φ.

$$p(a_{1,i}, a_{2,i}, \delta_i \mid \gamma, \varphi, I_1, I_2) = \left(\pi\, I_1\, I_2\, (1-\gamma^2)\right)^{-1} \times$$

$$2\, a_{1,i}\, a_{2,i} \exp\left(-\frac{I_2\, a_1^2 + I_1\, a_2^2 - 2 a_1\, a_2 \sqrt{I_1\, I_2}\, \gamma \cos(\delta_i - \varphi)}{I_1\, I_2 (1-\gamma^2)}\right) \quad (10)$$

The equation above is the general joint pdf of two correlated complex samples with individual expected intensities I_1 and I_2. As an example, Fig. 1 visualizes a likelihood function. A more specific joint PDF was published by Goodman [16].

$$p\left(a_{1,i}, a_{2,i}, \delta_i \mid \gamma, \varphi, \sigma = \sqrt{\frac{I_1}{2}} = \sqrt{\frac{I_2}{2}}\right) =$$

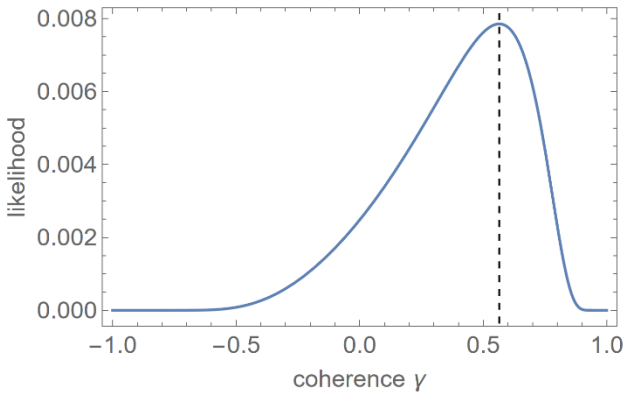

Fig. 1. Example likelihood from simulated data with N=3 and $\gamma = 0.3$ which results in the ML value $\hat{\gamma}_s = 0.56$.

$$\left(16\,\pi^2\,\sigma^4\,(1-\gamma^2)\right)^{-1} \exp\left(-\frac{a_1^2+a_2^2-2a_1\,a_2\,\gamma\,\cos(\delta_i-\varphi)}{2\,\sigma^2(1-\gamma^2)}\right) \quad (11)$$

This equation assumes equal intensities $I_1 = I_2$ and uses the standard deviation σ of the real and imaginary components as parameter. Straight forward to implement maximum likelihood (ML) estimators are known for (10) and (11). According to Touzi *et al.* [10], the sample coherence magnitude $\hat{\gamma}_s$ in (4) is the maximum likelihood (ML) estimate of the coherence magnitude γ. Seymour and Cumming [17] developed the ML estimator based on equation (11).

Equation (4) is universal. Therefore, it is often implemented in operational systems. However, this estimator is known to be biased, and the smaller the coherence, the more biased [18], [9]. The Bayesian framework is suitable for mitigating this situation as mentioned earlier [10]. A key element is the prior probability distribution $p(\gamma)$. In the conventional Bayesian framework, it is independent of the observed data. This work follows an empirical Bayes approach and the prior distribution is estimated from the data i.e. the sample estimator. This principle is explained first to clarify the development steps. Of course, a general hypothesis on the maximum coherence magnitude γ_{max} can be made. This information corresponds to a data independent prior and is established by a modification of the uninformative prior Bayes approach and is introduced subsequently.

A. Estimator with Uninformative Prior

The domain of the underlaying coherence is -1 to 1. Starting point is the prior $p(\gamma)$ in equation (5) which depends on the sample estimator outcome $\hat{\gamma}_s$. This is the reason, it is a conditional probability distribution $p(\gamma) = p(\gamma \mid \hat{\gamma}_s, N)$ expressing the underlying coherence γ probability given the sample estimate $\hat{\gamma}_s$ based on N sample pairs. It needs to include the available bias information. For the sample coherence estimator (4), Carter *et al.* [18] and Touzi and Lopez. [9] deduced the respective conditional probability distribution for $N > 2$ samples.

$$p(\hat{\gamma}_s \mid \gamma, N) = 2\hat{\gamma}_s\left(1-\hat{\gamma}_s{}^2\right)^{N-2}(N-1)\times (1-\gamma^2)^N\ {}_2F_1\left(N,N;1;\gamma^2\cdot\hat{\gamma}_s{}^2\right) \quad (12)$$

In the equation above, ${}_2F_1(.)$ is the Gaussian hypergeometric function. The product rule relates the joint PDF $p(\hat{\gamma}_s, \gamma \mid N)$ of the sample coherence $\hat{\gamma}_s$ and underlying coherence γ with equation (12).

$$p(\hat{\gamma}_s, \gamma \mid N) = p(\hat{\gamma}_s \mid \gamma, N)\cdot p_\gamma(\gamma \mid N) \quad (13)$$

The term $p_\gamma(\gamma \mid N)$ is the data independent prior and is simplified into $p_\gamma(\gamma)$ due to the independence of γ and N i.e. N has no effect on the true coherence γ and vice versa. For a generally applicable estimator, a uniform distribution $U(-1,1)$ i.e. a flat prior is selected for $p_\gamma(\gamma)$.

$$p_\gamma(\gamma) = U(-1,1) = \begin{cases} 1/2 & \text{for } -1 \le \gamma \le 1 \\ 0 & \text{otherwise} \end{cases} \quad (14)$$

In doing so, the joint PDF $p(\hat{\gamma}_s, \gamma \mid N)$ of $\hat{\gamma}_s$ and γ is proportional to the conditional probability distribution of the estimated coherence magnitude $\hat{\gamma}_s$ in equation (12).

$$p(\hat{\gamma}_s, \gamma \mid N) = \frac{1}{2}p(\hat{\gamma}_s \mid \gamma, N) \quad (15)$$

An example joint PDF of $\hat{\gamma}_s$ and γ is visualized in Fig. 2.

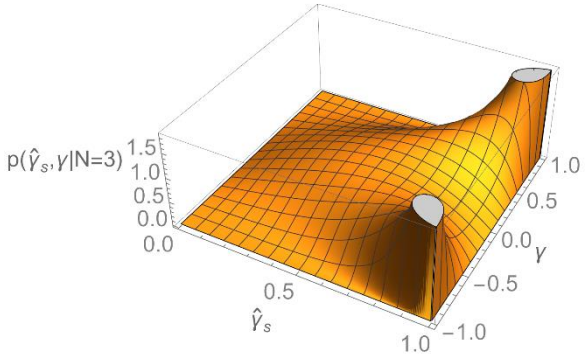

Fig. 2. Example joint probability density function of $\hat{\gamma}_s$ and γ i.e. $p(\hat{\gamma}_s, \gamma \mid N = 3)$

From the joint PDF $p(\hat{\gamma}_s, \gamma\,|N)$, the conditional probability distribution $p(\gamma \mid \hat{\gamma}_s, N)$ providing the empirical prior $p(\gamma)$ can be derived with Bayes' theorem.

$$p(\gamma) = p(\gamma \mid \hat{\gamma}_s, N) = \frac{p(\hat{\gamma}_s, \gamma\,|N)}{p(\hat{\gamma}_s \mid N)} \quad (16)$$

In the equation above, it is difficult to make assumptions about the term $p(\hat{\gamma}_s \mid N)$. It is the PDF of observing $\hat{\gamma}_s$ from N interferometric samples. Practically, for a posteriori based estimators, we are interested in a prior PDF $p(\gamma)$ which integrates to 1 whereas $p(\gamma \mid \hat{\gamma}_s, N)$ typically has not this characteristic. The following marginalization of $p(\hat{\gamma}_s, \gamma\,|N)$ with respect to γ makes the expression $p(\gamma)$ a valid PDF and comparison with (5) provides the PDF of observing $\hat{\gamma}_s$ given the number of samples.

$$p(\hat{\gamma}_s) = \int_{-1}^{1} p(\hat{\gamma}_s, \gamma|N)\,d\gamma = N!\sqrt{\pi}\,\hat{\gamma}_s(N-1)\left(1-\hat{\gamma}_s{}^2\right)^{N-2}\times {}_3F_2\left(\frac{1}{2},N,N;1,N+\frac{3}{2};\hat{\gamma}_s{}^2\right)/\,\Gamma\left(N+\frac{3}{2}\right) \quad (17)$$

In the equation above, $\Gamma(.)$ is the Euler gamma function. $p(\hat{\gamma}_s)$

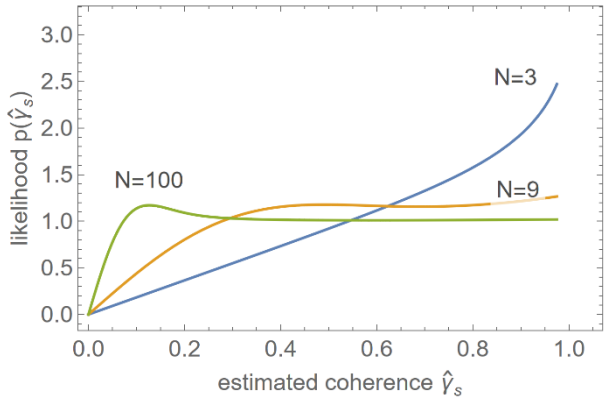

Fig. 3. PDF of observing the sample estimate $\hat{\gamma}_s$.

is plotted in Fig. 3 and the graphs correspond with the known characteristic of the sample coherence estimator. For N very small e.g. $N = 3$, the likelihood for large $\hat{\gamma}_s$ is higher than for each smaller $\hat{\gamma}_s$ because all sample estimates are biased towards higher coherence values. For $N = 9$, the plot shows a similar likelihood for sample estimates above 0.4. For N very large e.g. $N = 100$, the likelihood above 0.3 is similar. In fact, all graphs visualize the effect that small coherences are unlikely to be estimated due to the bias. The plot also shows, the larger the sample size, the smaller the coherence that can be reliably estimated. From (12) and (17), the empirical prior results.

$$p(\gamma) = p(\gamma \mid \hat{\gamma}_s, N) = \frac{(1-\gamma^2)^N \;\; {}_2F_1\left(N,N;1;\gamma^2\cdot{\hat{\gamma}_s}^2\right)\Gamma\left(N+\frac{3}{2}\right)}{\sqrt{\pi}\,N!\;\; {}_3F_2\left(\frac{1}{2},N,N;1,N+\frac{3}{2};{\hat{\gamma}_s}^2\right)} \tag{18}$$

The data dependent prior is in principle a bimodal PDF which becomes unimodal for small $\hat{\gamma}_s$ and is visualized in Fig. 4. With (9) and (18), the posterior distribution (5) is practically evaluated by

$$\begin{aligned} &p\left(\gamma \mid a_{1,i=1}, a_{2,i=1}, \delta_{i=1}, \dots, a_{1,i=N}, a_{2,i=N}, \delta_{i=N}, \hat{\gamma}_s, \hat{\varphi}_s, N\right) = \\ &\quad \frac{1}{m}\cdot(1-\gamma^2)^N \;\; {}_2F_1\left(N,N;1;\gamma^2\cdot{\hat{\gamma}_s}^2\right)\Gamma\left(N+\frac{3}{2}\right)\times \\ &\quad \left(\sqrt{\pi}\,N!\;\; {}_3F_2\left(\frac{1}{2},N,N;1,N+\frac{3}{2};{\hat{\gamma}_s}^2\right)\right)^{-1}\times \\ &\quad \prod_{i=1}^{N} p\left(a_{1,i}, a_{2,i}, \delta_i \mid \gamma, I_1, I_2, \hat{\varphi}_s\right). \end{aligned} \tag{19}$$

The evidence i.e. the marginal likelihood $m = \int_{\gamma=-1}^{1} p(\gamma \mid x_1, \dots, x_N, \hat{\gamma}_s, N)\, p(\gamma)\, d\gamma$ is not needed for the coherence estimation by the maximum and median a posteriori principle. However, for the expected a posteriori method, it is straight forward implemented within the expected value calculation. It is only needed once for the calculation of this value and a numerical integration works without any problems.

B. Estimator with Informative Prior

The principle of the estimator with uninformative prior is extended. Two general priors are designed to express practically available information. Firstly, a strict maximum underlaying coherence γ_{max} is assumed e.g. by knowing the best possible primary and secondary SNRs from the relation $\gamma_{max} = \left(1 + 1/SNR_1\right)^{0.5} \cdot \left(1 + 1/SNR_2\right)^{0.5}$ [19].

$$\begin{aligned} p_\gamma(\gamma) &= U(-\gamma_{max}, \gamma_{max}) \\ &= \begin{cases} 1/(2\gamma_{max}) & \text{for } -\gamma_{max} \le \gamma \le \gamma_{max} \\ 0 & \text{otherwise} \end{cases} \end{aligned} \tag{20}$$

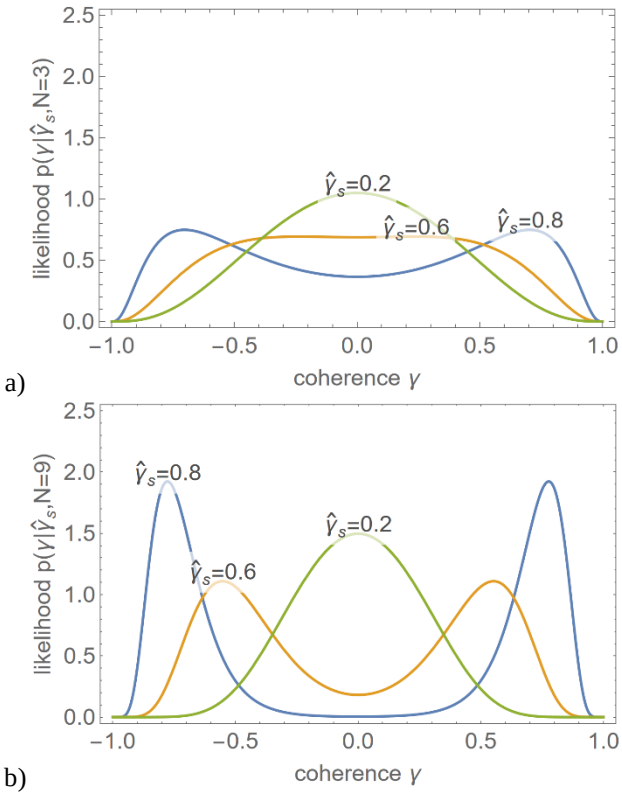

Fig. 4. Example empirical priors based on an uninformative general prior (a) $N = 3$, (b) $N = 9$.

Secondly, a less strict maximum underlaying coherence γ_{max} is assumed e.g. a maximum coherence is known from many measurements. For InSAR based on time series, this is a typical situation with data stacks covering more than a decade. A linearly decreasing function outside of the assumed range makes the prior less strict.

$$p_\gamma(\gamma) = \begin{cases} \frac{1}{\gamma_{max}+1} & \text{for } -\gamma_{max} \le \gamma \le \gamma_{max} \\ \frac{\gamma}{1-\gamma_{max}^2} + \frac{1}{1-\gamma_{max}^2} & \text{for } -1 \le \gamma < -\gamma_{max} \\ \frac{-\gamma}{1-\gamma_{max}^2} + \frac{1}{1-\gamma_{max}^2} & \text{for } \gamma_{max} < \gamma \le 1 \\ 0 & \text{otherwise} \end{cases} \tag{21}$$

Both general priors are visualized in Fig. 5.

In order to get the data dependent prior $p(\gamma)$ equivalent to (16), the joint probability $p(\gamma, \hat{\gamma}_s) = p(\hat{\gamma}_s|\gamma)\, p_\gamma(\gamma)$ needs to be evaluated. This is straight forward implemented with (12) and (20) or (21). However, the respective marginalization integral over γ for the normalization $p(\hat{\gamma}_s)$ cannot be solved directly and numerical integration in a later calculation step works well. It needs to be evaluated once per estimation and can be computed together with the overall normalization (i.e. evidence) which is finally needed for the a posteriori PDF. Analogous to (19) which describes the general situation, the posterior distribution for the more informative prior $p_\gamma(\gamma)$ is

$$\begin{aligned} &p\left(\gamma \mid a_{1,i=1}, a_{2,i=1}, \delta_{i=1}, \dots, a_{1,i=N}, a_{2,i=N}, \delta_{i=N}, \hat{\gamma}_s, \varphi_s, N\right) \\ &\quad = \frac{p(\hat{\gamma}_s \mid \gamma)\cdot p_\gamma(\gamma)}{m} \cdot \prod_{i=1}^{N} p\left(a_{1,i}, a_{2,i}, \delta_i \mid \gamma, I_1, I_2, \varphi_s\right) \end{aligned} \tag{22}$$

For the evidence i.e. the marginal likelihood $m =$

$\int_{\gamma=-1}^{1} p(\gamma \mid x_1, \ldots, x_N, \hat{\gamma}_s, N)\, p(\gamma)\, d\gamma$, a numerical integration is fine.

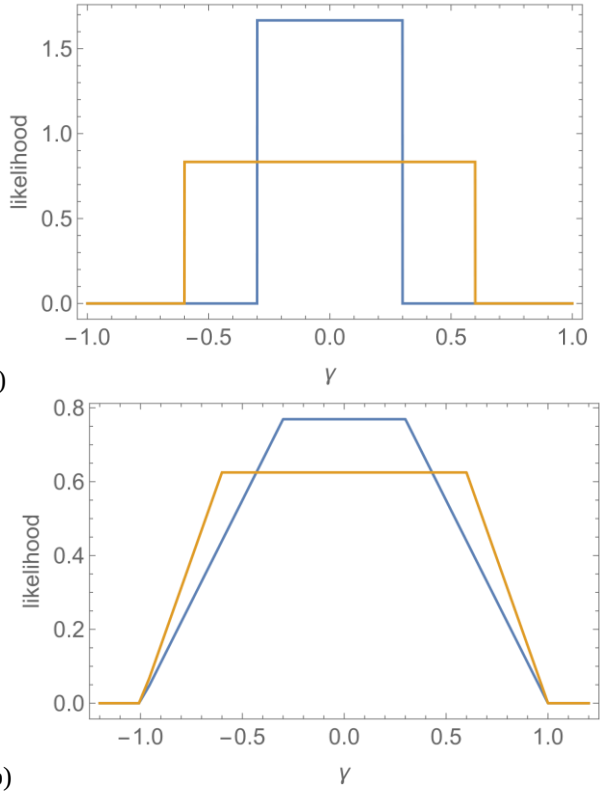

Fig. 5. General informative prior: $\gamma_{max} = 0.3$, $\gamma_{max} = 0.6$; (a) strict prior (b) less strict prior.

C. Implementation Hints

For the implementation of the Bayesian methods, the posterior distribution $p(\gamma \mid D)$ in (6), (7) or (8) is substituted with (19) or (22). Equation (6) is implemented by a numerical one-dimensional maximization with the constraint $0 \leq \hat{\gamma}_{MAP} \leq \gamma_{max}$. For the uninformative and the less strict prior is $\gamma_{max} = 1$. The respective implementation is straight forward as the posterior distribution is unimodal in the range $0 - 1$. In practice, (7) is implemented by numerical integration $\hat{\gamma}_{EAP} = \int_{-\gamma_{max}}^{\gamma_{max}} \gamma\, p(\gamma \mid D)\, d\gamma$ with the evidence m pulled out of the integral as a constant. Furthermore, (8) can be implemented by bisection on the left and right areas separated by $\hat{\gamma}_{MEDAP}$ under the posterior distribution. This is the reason, the marginal m is not relevant for the median computation.

In the author's implementation, the hypergeometric functions ${}_2F_1(.)$ and ${}_3F_2(.)$ are not computed directly but the respective logarithms due to the wide function range. For the operational implementation, lookup tables are coded for specific N with interpolation of intermediate points for each function. Of course, the log probabilities are used for the computation of the product and ratio of probabilities.

III. Results

The characteristics of the estimators are evaluated numerically by simulations without simplification or modelling. All estimators are applied on one and the same simulated samples from CCG processes. Because of its practical importance, the conventional sample estimator $\hat{\gamma}_s$ (4) is taken as the reference and included in the comparison of the estimators. In practice, the coherence bias is extreme when the sample size is small. This is the reason, these problematic scenarios are given priority in the assessment. In the subsections below, the sample sizes $N = 3$ and $N = 9$ are characterized in detail over the range 0 – 0.95 of coherences in steps of 0.05 plus an extra simulation with coherence 0.98. In order to estimate the bias $\gamma_{bias} = E\{\hat{\gamma}_* - \gamma_{true}\}$, the estimator standard deviation $\gamma_\sigma = \sqrt{E\{(\hat{\gamma}_* - E\{\hat{\gamma}_*\})^2\}}$ and the root mean square error (RMSE) $\gamma_{rmse} = \sqrt{E\{(\hat{\gamma}_* - \gamma_{true})^2\}}$ for $\{\hat{\gamma}_* | \hat{\gamma}_s, \hat{\gamma}_{MAP}, \hat{\gamma}_{EAP}, \hat{\gamma}_{MEDAP}, \hat{\gamma}_{MAPSP}, \hat{\gamma}_{MAPLSP}\}$, 10^6 draws are generated for each sample size with a specific underlaying coherence. In this paper, the RMSE is used instead of the mean square error (MSE) for the characterization of the estimator efficiency because this parameter is in the same scale as the true coherence.

A. Estimator Characteristic with Uninformative Prior, N=3

Firstly, normalized histograms are presented to show the distribution of the estimated coherence depending on the underlaying true coherence. Each histogram below is estimated from 10^6 simulations and visualized with 200 bins.

The histograms in Fig. 6 show, that all Bayesian estimators reduce the estimation likelihood around high coherences compared to the conventional sample estimator. Plot (a) demonstrates that the Bayesian estimators increase the likelihood around the given coherence of 0.15. This is the reason, a reduced bias for small coherences is an expected characteristic. Plot (b) shows that the EAP and MEDAP methods distribute the estimates more evenly for the given coherence of 0.5 compared to the conventional sample estimator and the MAP. In contrast, the sample and the MAP estimator prefer higher coherences and a larger bias for small coherences results. Therefore, a small bias is expected for both estimators around a coherence of 0.5. Plot (c), visualizes the distribution of the estimates for a true coherence of 0.8. The Bayesian estimators reduce the overestimation, but distribute more estimates towards lower coherences which are further away from the true value. This characteristic has an adverse impact on the bias and the RMSE.

The reduced bias for small coherences is confirmed by plot (d) in Fig. 6 which visualizes the bias of each estimator. For a zero coherence, the bias is reduced from 0.534 to 0.356 (33.3%) for the EAP, to 0.385 (27.8%) for the MEDAP and to 0.454 (14.9%) for the MAP estimator. Besides, for the sample estimator, the bias becomes zero at a given coherence of one. All newly developed estimators, are bias free at much smaller coherences. The EAP is bias free around a true coherence of 0.46, the MEDAP around 0.54 and the MAP around 0.8. However, the bias becomes notably negative for the EAP and MEDAP estimators afterwards. As will be shown later, this characteristic has an adverse impact on the estimator performance expressed by the RMSE. Plot (e) compares the estimator standard deviations. The standard estimator has the

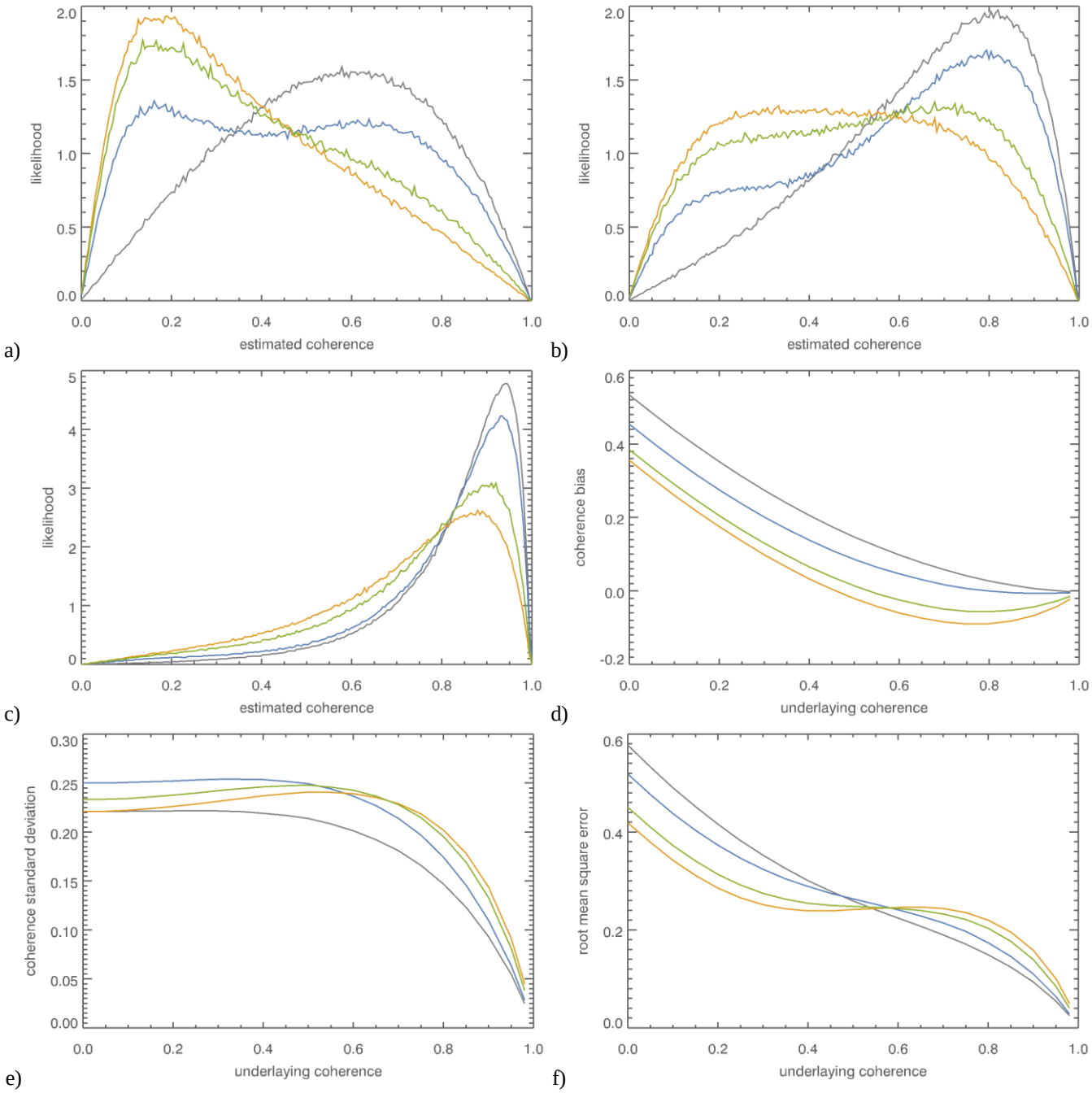

Fig. 6. Characteristic of estimators for 3 looks; ■ sample estimator, ■ MAP, ■ EAP, ■ MEDAP each with uninformative prior
a) Histograms of estimates with true coherence $\gamma = 0.15$
b) Histograms of estimates with true coherence $\gamma = 0.5$
c) Histograms of estimates with true coherence $\gamma = 0.8$
d) Estimation bias γ_{bias}
e) Standard deviation γ_{σ}
f) Root mean square error γ_{rmse}.

smallest values over the entire range and the EAP estimator is comparably good up to a coherence about 0.1.

Fig. 6 (f) visualizes the performance characteristic of the estimators for $N = 3$. The root mean square error includes the bias and the variance γ_σ^2 of the estimators because $\gamma_{rmse} = \sqrt{\gamma_{bias}^2 + \gamma_\sigma^2}$. In particular, EAP is more efficient compared to the conventional sample estimator for all underlaying coherences up to 0.54, the MEDAP method up to 0.53 and the MAP estimator up to 0.47.

B. Estimator Characteristic with Uninformative Prior, N=9

The characteristic of $N = 9$ is similar to the test case with 3 looks and confirms the principle of improvements. Likewise, the histograms in Fig. 7 show that all Bayesian estimators reduce the estimation likelihood around high coherences compared to the conventional sample estimator.

The reduced bias for small coherences is confirmed by plot (d) which visualizes the bias of each estimator. For a zero coherence, the bias is reduced from 0.3 to 0.212 (29.1%) for the EAP, to 0.223 (25.7%) for the MEDAP and to 0.245 (18.1%) for the MAP estimator. Again, for the sample estimator, the bias becomes zero at a true coherence of one. All newly developed estimators, are bias free at much smaller coherences as well compared to the setup with $N = 3$. The EAP is bias free around a true coherence of 0.34, the MEDAP around 0.39 and the MAP around 0.65. Plot (e) compares the estimator standard deviations. Now, the EAP estimator is better than the sample estimator in the coherence interval from 0 – 0.16. The standard estimator has the smallest values over the remaining coherence interval.

Fig. 7 (f) visualizes the overall performance characteristic for each estimator with N=9. The EAP and the MEDAP methods are more efficient compared to the conventional sample estimator for all underlaying coherences up to 0.37 and 0.36 accordingly. And the MAP is more efficient for true coherences up to 0.31.

C. Estimator Characteristic with Informative Prior, N=3

The previous subsections have demonstrated that the EAP estimator performs best compared to MAP and MEDAP estimators. For the sake of conciseness, this method is presented for the informative prior (i.e. the strict und less strict prior) and is compared with the conventional sample estimator and the newly develop EAP estimator with uninformative prior. As an example, the maximum underlaying coherence is set to $\gamma_{max} = 0.6$. The respective general priors are plotted in orange in Fig. 5. Fig. 8 (a) and (b) show, that the estimator $\text{EAPSP}_{0.6}$ with strict prior succeeds to keep all values within the pre-set range. This is the reason, a reduced bias and standard deviation are expected characteristics. However, it is noticeable that this method only returns values below 0.5 instead within the full range 0 – 0.6. The less strict estimator $\text{EAPLSP}_{0.6}$ returns estimates in the full range from 0 – 1 and prioritizes values in the prior range 0 – 0.6 compared to the uninformative EAP estimator.

The reduced bias for small coherences is confirmed by plot (d) in Fig. 8 which visualizes the bias of each estimator. For a zero coherence, the bias is reduced from 0.534 to 0.26 (51.3%) for the $\text{EAPSP}_{0.6}$, to 0.338 (36.6%) for the $\text{EAPLSP}_{0.6}$ and to 0.356 (33.3%) for the EAP estimator with uninformative prior.

For the sample estimator, the bias becomes zero at a true coherence of one. Once again, all newly developed estimators, are bias free at much smaller coherences as well compared to the uninformative setup with $N = 3$. The $\text{EAPSP}_{0.6}$ is bias free around a true coherence of 0.27, the $\text{EAPLSP}_{0.6}$ around 0.42 and the EAP around 0.46. Plot (e) compares the estimator standard deviations. For a zero coherence, the estimation standard deviation is reduced from 0.221 to 0.122 (44.7%) for the $\text{EAPSP}_{0.6}$, to 0.203 (8%) for the $\text{EAPLSP}_{0.6}$ and to 0.221 (0.02%) for the EAP estimator with uninformative prior. For the strict informative prior, the estimation standard deviation is always smaller compared to the sample estimator. The less strict informative prior is better than the sample estimator in the coherence interval from 0 – 0.42.

Fig. 8 (f) visualizes the total performance characteristic for each estimator with $N = 3$. The $\text{EAPSP}_{0.6}$ and the $\text{EAPLSP}_{0.6}$ methods are more efficient compared to the conventional sample estimator and to the EAP with uninformative prior for nearly all underlaying coherences in the prior range. Only the small coherence ranges from 0.55 – 0.6 for $\text{EAPSP}_{0.6}$ and 0.57 – 0.6 for $\text{EAPLSP}_{0.6}$ are worse in terms of performance.

D. Estimator Characteristic with Informative Prior, N=9

Once again, the maximum underlaying coherence is set to $\gamma_{max} = 0.6$ as an example. Fig. 9 (a) and (b) show, that the estimator $\text{EAPSP}_{0.6}$ with strict prior succeeds to keep all values within the pre-set range and prioritizes values around the true coherence. These are the reasons, a reduced bias and standard deviation are also expected characteristics. It is noticeable that this method only returns values below 0.57 instead within the full range 0 - 0.6. However, this range is larger compared to the test case with $N = 3$ looks which is 0 - 0.5. The less strict estimator $\text{EAPLSP}_{0.6}$ returns estimates in the full range from 0 - 1 and has always a similar or higher likelihood in the prior range 0 - 0.6 compared to the uninformative EAP estimator.

The reduced bias for small coherences is confirmed by plot (d) in Fig. 9 which visualizes the bias of each estimator. For a zero coherence, the bias is reduced from 0.3 to 0.205 (31.5%) for the $\text{EAPSP}_{0.6}$, to 0.212 (29.4%) for the $\text{EAPLSP}_{0.6}$ and to 0.212 (29.1%) for the EAP estimator with uninformative prior.

For the sample estimator, the bias becomes zero at a true coherence of one. Once again, all newly developed estimators, are bias free at much smaller coherences as well compared to the informative prior and $N = 3$ looks. The $\text{EAPSP}_{0.6}$ is bias free around a true coherence of 0.27, the $\text{EAPLSP}_{0.6}$ around 0.32 and the EAP around 0.33. Plot (e) compares the estimator standard deviations. For a zero coherence, the estimation standard deviation is reduced from 0.146 to 0.129 (11.8%) for the $\text{EAPSP}_{0.6}$, to 0.141 (3.8%) for the $\text{EAPLSP}_{0.6}$ and to 0.142 (2.7%) for the EAP estimator with uninformative prior. For the strict informative prior, the estimation standard deviation is always smaller compared to the sample estimator. The less strict informative prior is better than the sample estimator in the coherence interval from 0 – 0.2.

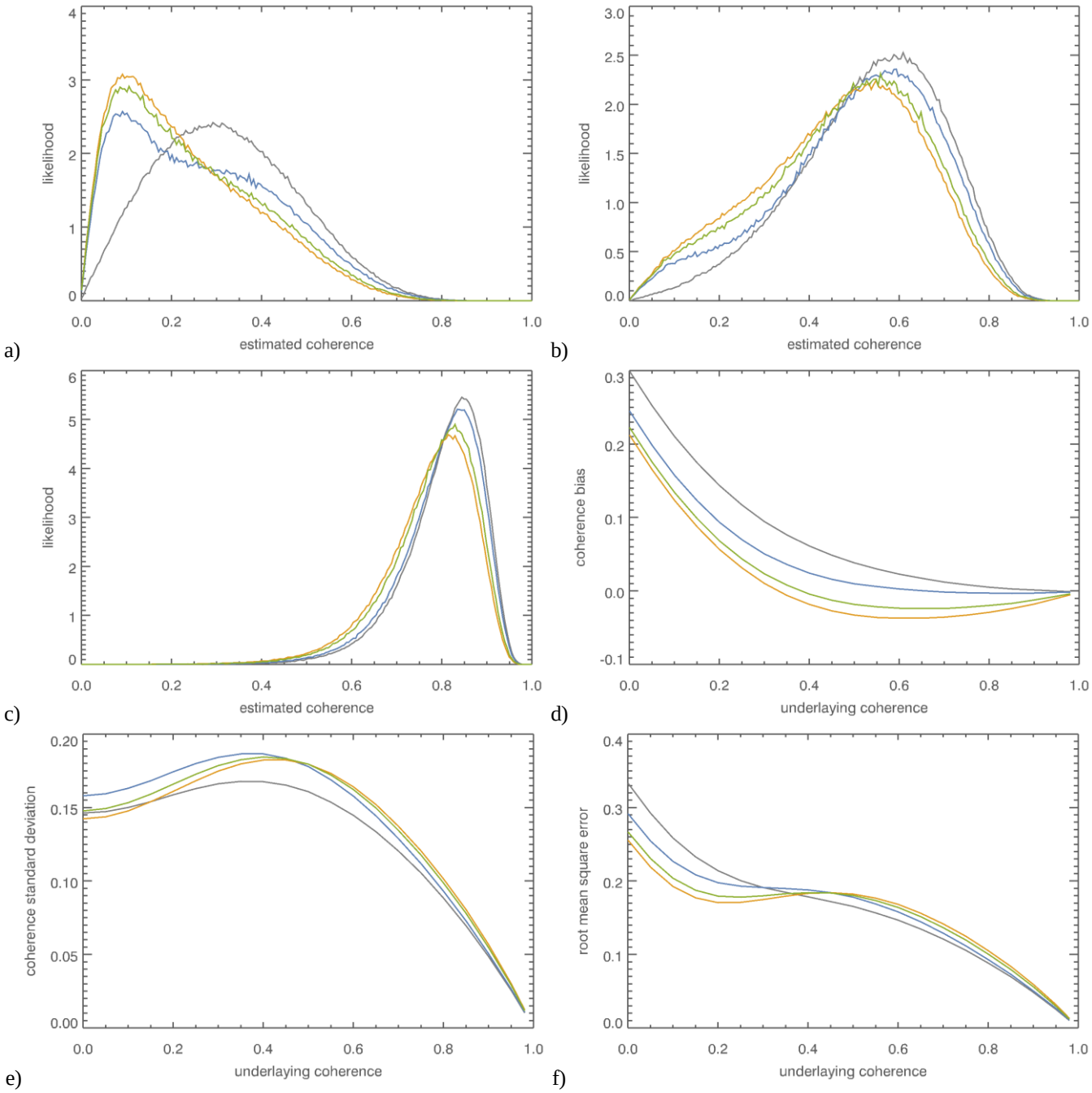

Fig. 7. Characteristic of estimators for 9 looks; ■ sample estimator, ■ MAP, ■ EAP, ■ MEDAP each with uninformative prior
a) Histograms of estimates with true coherence $\gamma = 0.15$
b) Histograms of estimates with true coherence $\gamma = 0.5$
c) Histograms of estimates with true coherence $\gamma = 0.8$
d) Estimation bias γ_{bias}
e) Standard deviation γ_{σ}
f) Root mean square error γ_{rmse}.

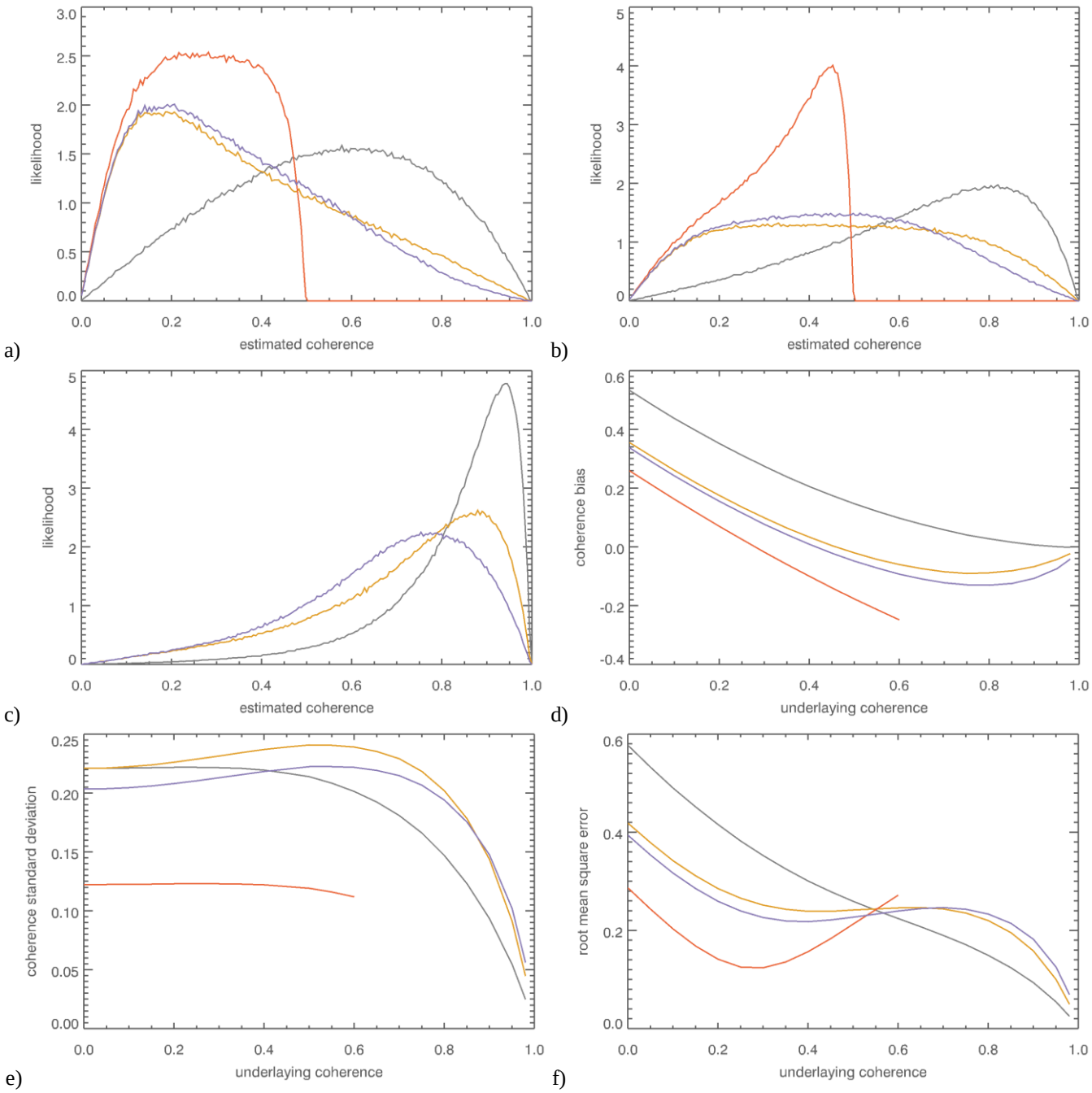

Fig. 8. Characteristic of estimators for 3 looks; ■ sample estimator, ■ EAP, ■ $EAPSP_{0.6}$, ■ $EAPLSP_{0.6}$
a) Histograms of estimates with true coherence $\gamma = 0.15$
b) Histograms of estimates with true coherence $\gamma = 0.5$
c) Histograms of estimates with true coherence $\gamma = 0.8$
d) Estimation bias γ_{bias}
e) Standard deviation γ_{σ}
f) Root mean square error γ_{rmse}.

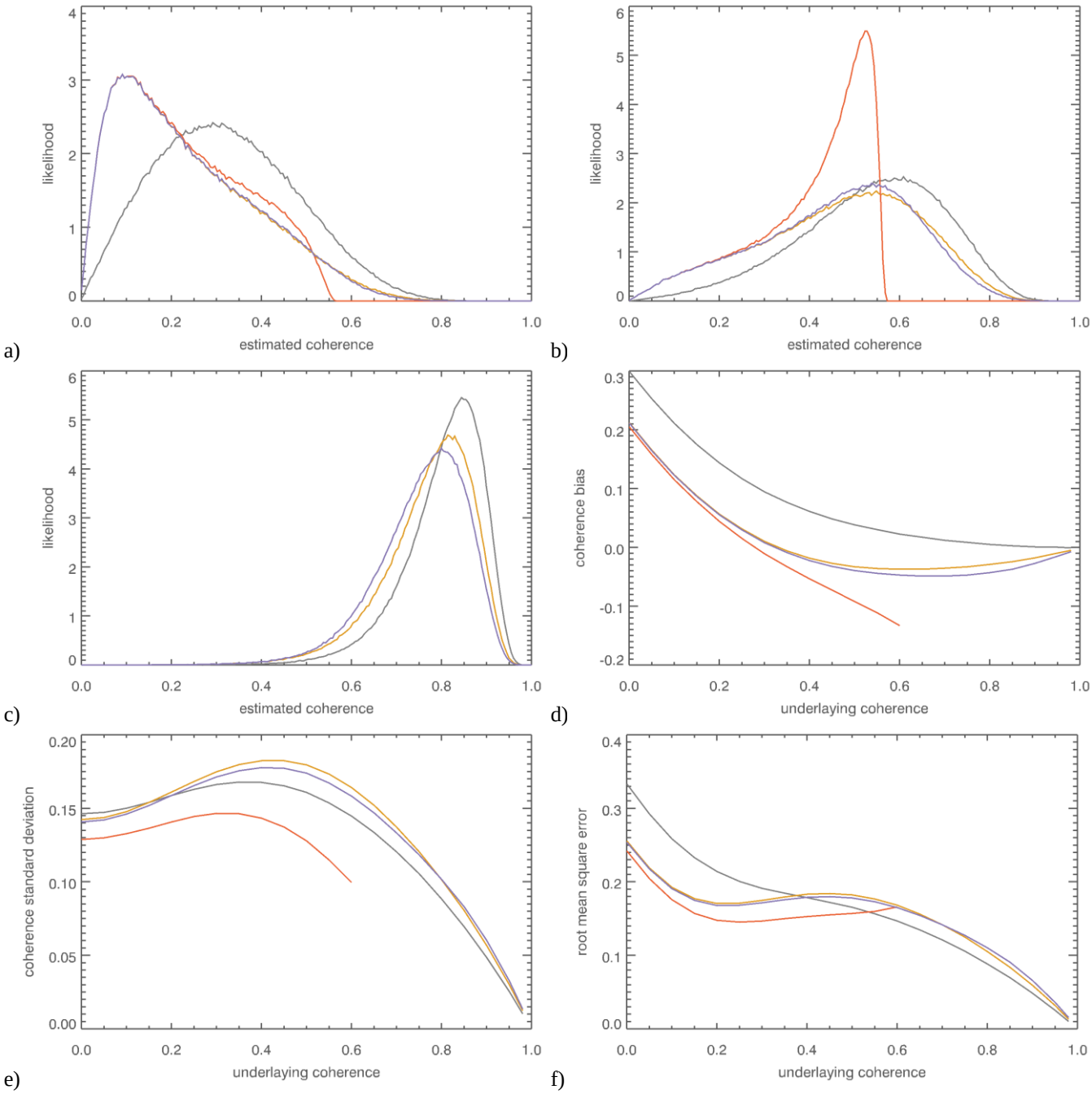

Fig. 9. Characteristic of estimators for 9 looks; ■ sample estimator, ■ EAP, ■ $EAPSP_{0.6}$, ■ $EAPLSP_{0.6}$
a) Histograms of estimates with true coherence $\gamma = 0.15$
b) Histograms of estimates with true coherence $\gamma = 0.5$
c) Histograms of estimates with true coherence $\gamma = 0.8$
d) Estimation bias γ_{bias}
e) Standard deviation γ_{σ}
f) Root mean square error γ_{rmse}.

Fig. 9 (f) visualizes the performance characteristic for each estimator with $N = 9$ looks. The $\mathrm{EAPSP}_{0.6}$ method is more efficient compared to the conventional sample estimator in the complete general prior interval. And the $\mathrm{EAPLSP}_{0.6}$ is more efficient for true coherences up to 0.4.

IV. Discussion

The developed empirical Bayesian estimators provide two main advantages compared to the conventional sample estimator. All improve the estimation of small coherences. And, they better estimate the coherence from small sample sizes. The expected a posteriori method performs better (see Fig. 6 and Fig. 7) compared to the median and maximum a posteriori estimator. Using an informative prior, the bias and the standard deviation continue to decrease for small coherences. The strict general prior achieves the best performance with respect to the RMSE. The mode, median and mean of the posterior distribution $p(\gamma \mid D)$ result in different biases due to the skewness of this distribution. For the bias, the simulation demonstrates that EAP < MEDAP < MAP always applies. In principle, this order results from the negative skew of the posterior distribution.

In principle, all estimators are suitable for typical InSAR scenarios. Firstly, the uninformative general prior improves the estimation without prior knowledge and is generally applicable. Secondly, the informative general priors include an assumption on the maximum coherence of the underlaying coherence. Indeed, such information is available in SAR interferometry based on time series. The strict prior limits the estimates inside the assumed range and the less strict prior favors estimates in this range.

Equation (12) is valid for $N > 2$ samples as shown by Touzi *et al.* [10]. It is a well-known fact, the concept of coherence is not relevant to individual samples. However, a typical situation in PSI requires the coherence estimate of only two samples as mentioned already by Ferretti *et al.* in figure 4 of [5]. The simulation of the test case with $N = 2$ has shown that all developed methods also work very well in this setup. This is the reason, the corresponding results are included in the performance plots although not directly supported by equation (12). Fig. 10 presents for $N = 2$ the bias, standard deviation and RMSE for the estimators with uninformative (left column) and informative (right column) general priors. Comparing the RMSE, especially the informative general priors are recommended for the estimation with only two samples.

An unexpected result is the reduced estimation range of the estimator with strict prior. In the presented test cases (see plots (a) and (b) in Fig. 8 and Fig. 9), the strict prior excludes coherence estimates close to the end of the general prior interval γ_{max}. This effect reduces with increasing number of samples. In practice, it can be mitigated by increasing the general prior γ_{max} by a small amount.

For $N = 8$ samples, Fig. 11 demonstrates the bias, standard deviation and the RMSE for the uninformative and informative prior respectively. Corresponding characterizations are provided by Jiang *et al.* [13] in figures 5 (a) and 6 (a). For a zero underlaying coherence, an example for reading the values from the respective plots is provided in table I. The rows are sorted for the RMSE i.e. the estimator efficiency. For the specific test case $N = 8$, the double bootstrap method has the smallest bias of the compared estimators. However, Jiang *et al.* [13] inform that the double bias correction introduces more variability which is evident in column 2 of table I and finally in the estimator efficiency (RMSE). Only when the underlaying coherence is greater than 0.66, the standard deviations are of the same order of magnitude.

TABLE I
EXAMPLE FOR USE OF PLOTS ($\gamma = 0$)

	Bias γ_{bias}	Std. Dev. γ_{σ}	RMSE
$\mathrm{EAPSP}_{0.6}$	0.218	0.131	0.25
$\mathrm{EAPLSP}_{0.6}$	0.220	0.146	0.27
EAP	0.22	0.15	0.27
MEDAP	0.235	0.155	0.28
MAP	0.26	0.167	0.31
Double Bootstrap	0.184	0.254	0.314
Sample Estimator	0.32	0.154	0.35

For comparison with other methods e.g. from Abdelfattah and Nicolas [12] and Touzi *et al.* [10], Fig. 12 provides the characteristic of the Bayesian estimators for $N = 10$. One reviewer has pointed out that the second kind statistical estimator [12] and coherence magnitude estimation from complex coherence maps [10] need M i.i.d. coherence samples to mitigate the bias and standard deviation. These additional samples are not available in typical InSAR applications and render these methods impractical. The developed empirical Bayesian estimators have no such limitation.

Above, the advantage of the Bayesian methods is demonstrated for small sample sizes. The characterization for large sample sizes is provided for $N = 15$ in Fig. 13, $N = 30$ in Fig. 14 and $N = 60$ in Fig. 15. These examples show that even for large N, the bias of all methods is always smaller than the sample estimator's and still becomes negative. However, as the sample size increases, the bias vanishes and the estimators are also asymptotically unbiased. All Bayesian estimators except EASP_{06} approach to a similar bias, standard deviation and RMSE characteristic. Especially, the RMSE indicates that the Bayes methods can be recommended for all sample sizes $N \geq 15$. It is noteworthy that the strict prior performs best also with large sample sizes.

A limitation of the newly developed methods is that the performance improves only for low coherences if the sample size is small. For the estimators with uninformative prior, the threshold $\gamma_{threshold}$ from when the conventional sample estimator should be used is shown in Fig. 16 and provided in table II. The test case of an informative prior with $\gamma_{max} = 0.6$ is presented in Fig. 17. In this figure, the range above 0.6 is excluded by the strict general prior. Table III provides the limits of the informative prior compared to the sample estimator.

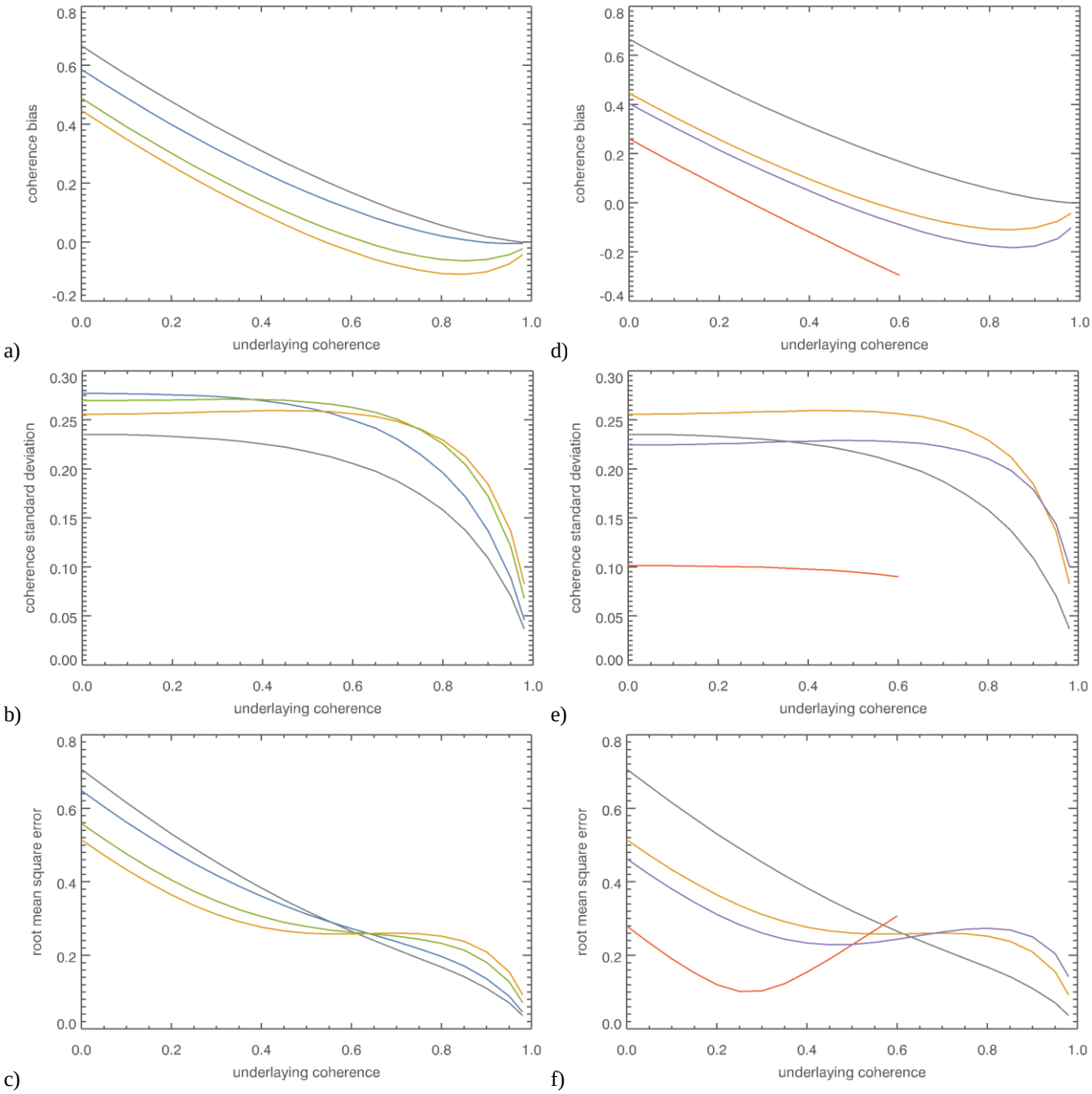

Fig. 10. Characteristic of estimators for 2 looks;
left column provides the uninformative prior and the right column the informative prior;
■ sample estimator, ■ MAP, ■ EAP, ■ MEDAP each with uninformative prior,
■ $EAPSP_{0.6}$, ■ $EAPLSP_{0.6}$ both have an informative prior
a) and d) Estimation bias γ_{bias}
b) and e) Standard deviation γ_{σ}
c) and f) Root mean square error γ_{rmse}

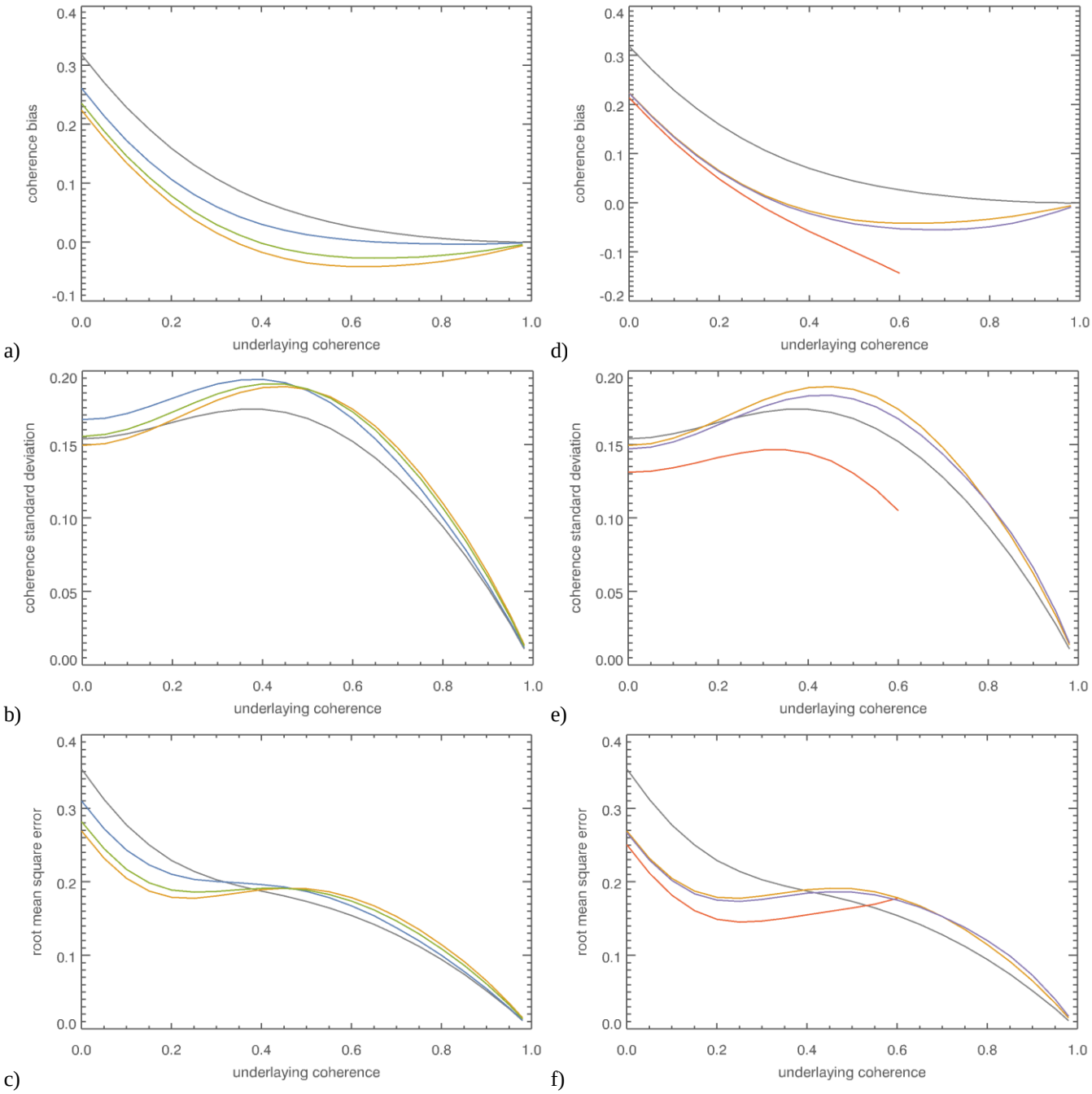

Fig. 11. Characteristic of estimators for 8 looks;
left column provides the uninformative prior and the right column the informative prior;
■ sample estimator, ■ MAP, ■ EAP, ■ MEDAP each with uninformative prior,
■ $EAPSP_{0.6}$, ■ $EAPLSP_{0.6}$ both have an informative prior
a) and d) Estimation bias γ_{bias}
b) and e) Standard deviation γ_{σ}
c) and f) Root mean square error γ_{rmse}

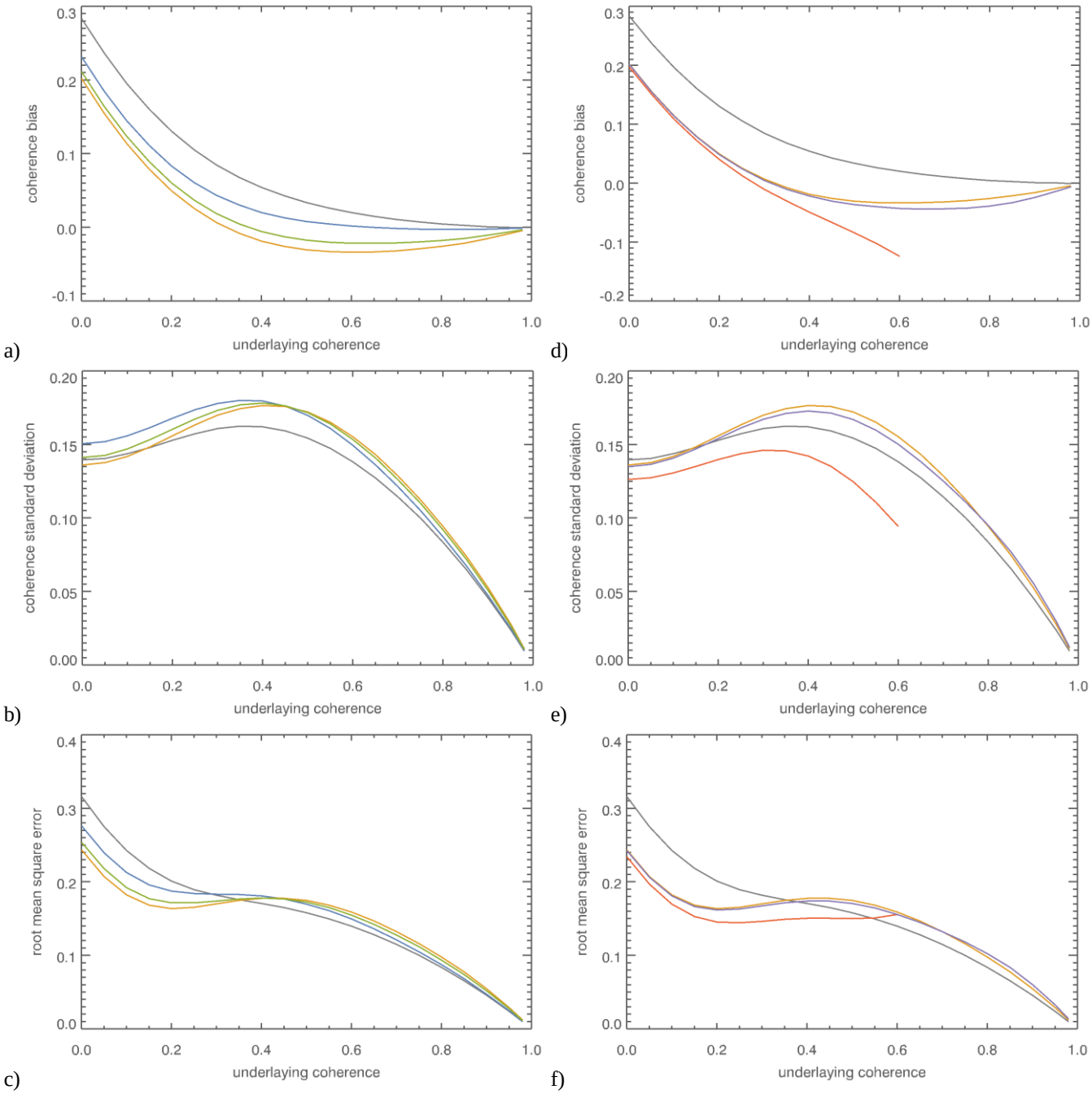

Fig. 12. Characteristic of estimators for 10 looks;
left column provides the uninformative prior and the right column the informative prior;
■ sample estimator, ■ MAP, ■ EAP, ■ MEDAP each with uninformative prior,
■ $EAPSP_{0.6}$, ■ $EAPLSP_{0.6}$ both have an informative prior
a) and d) Estimation bias γ_{bias}
b) and e) Standard deviation γ_{σ}
c) and f) Root mean square error γ_{rmse}

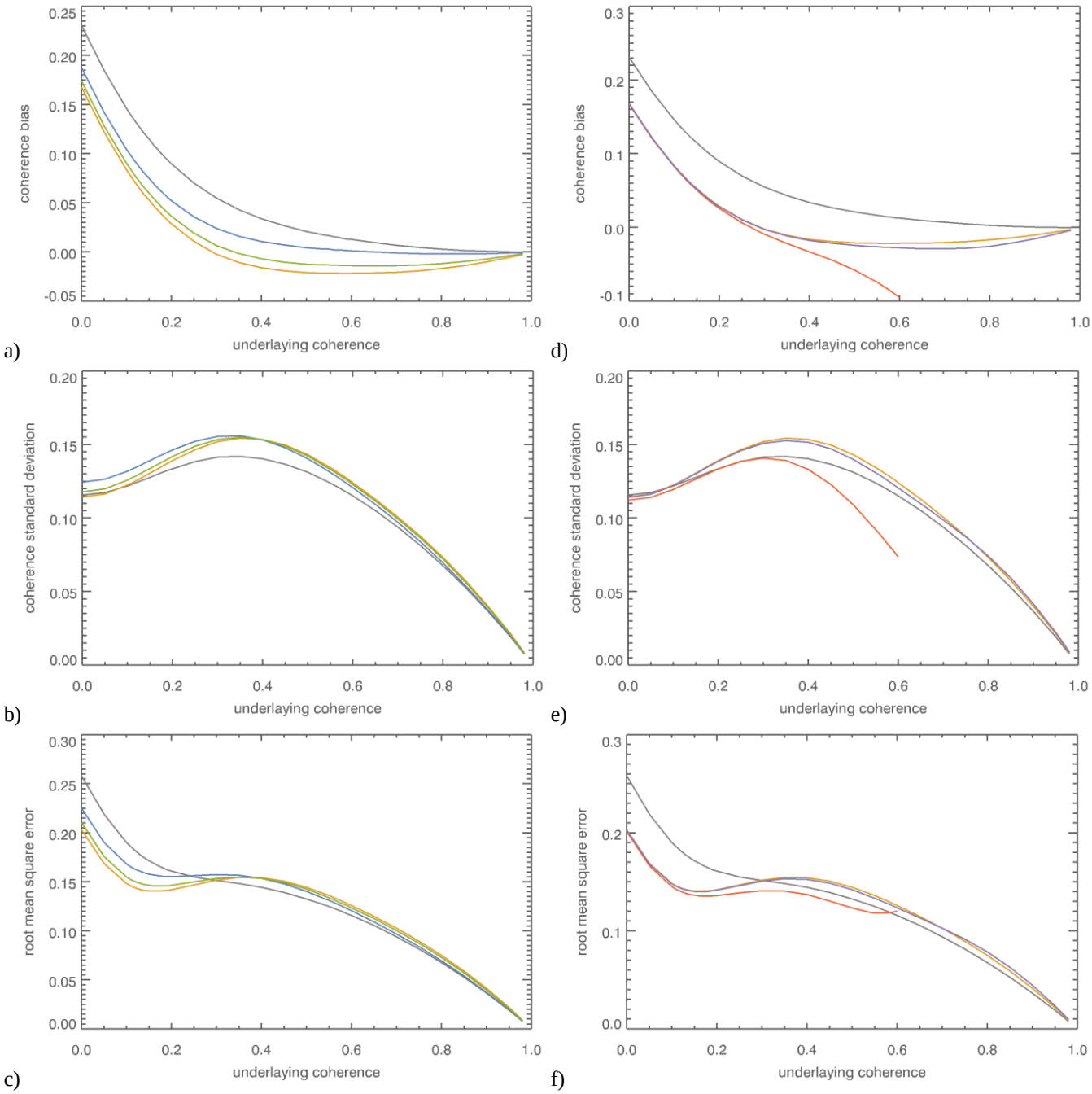

Fig. 13. Characteristic of estimators for 15 looks;
left column provides the uninformative prior and the right column the informative prior;
■ sample estimator, ■ MAP, ■ EAP, ■ MEDAP each with uninformative prior,
■ $EAPSP_{0.6}$, ■ $EAPLSP_{0.6}$ both have an informative prior
a) and d) Estimation bias γ_{bias}
b) and e) Standard deviation γ_{σ}
c) and f) Root mean square error γ_{rmse}

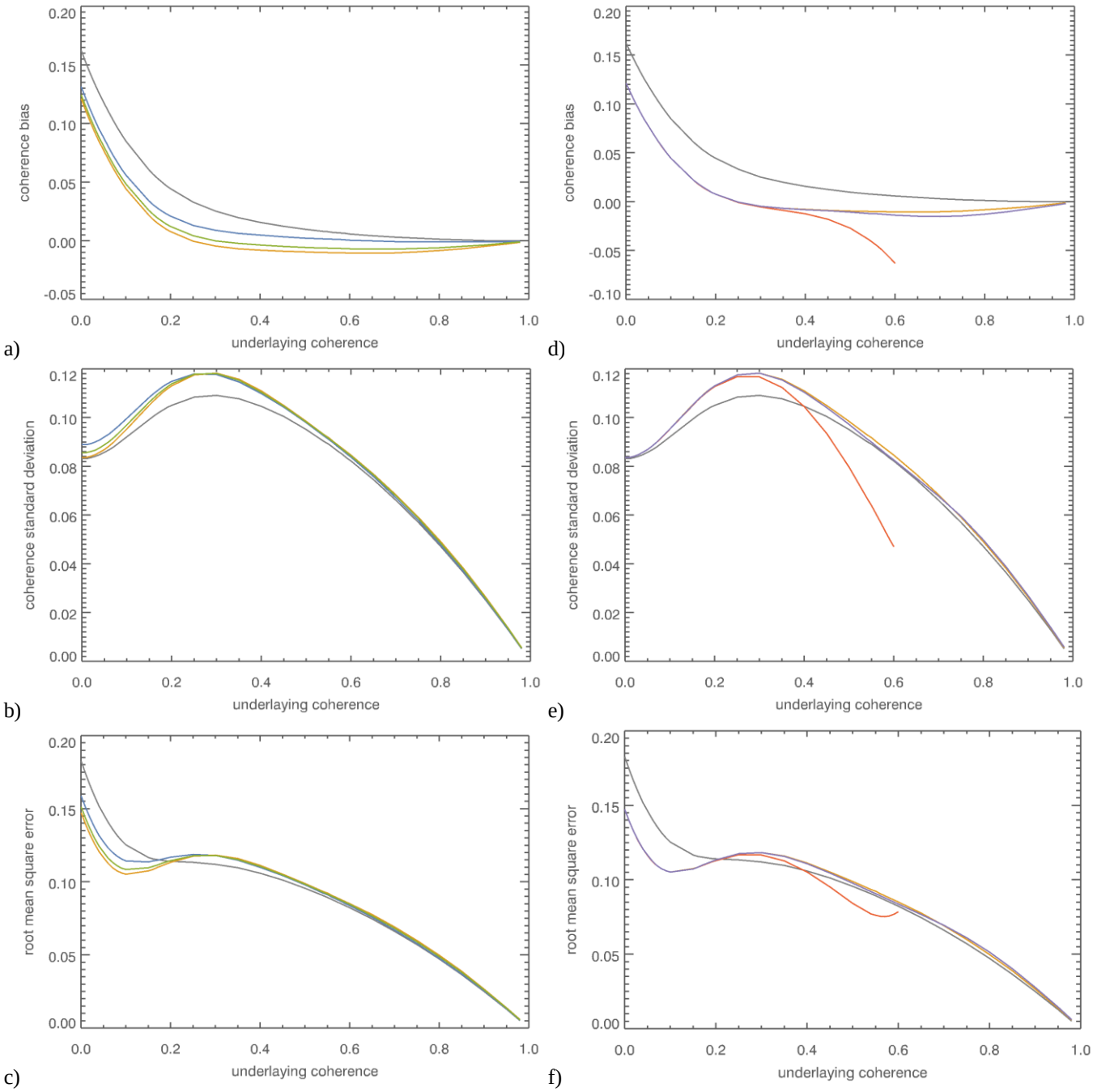

Fig. 14. Characteristic of estimators for 30 looks;
left column provides the uninformative prior and the right column the informative prior;
■ sample estimator, ■ MAP, ■ EAP, ■ MEDAP each with uninformative prior,
■ $EAPSP_{0.6}$, ■ $EAPLSP_{0.6}$ both have an informative prior
a) and d) Estimation bias γ_{bias}
b) and e) Standard deviation γ_{σ}
c) and f) Root mean square error γ_{rmse}

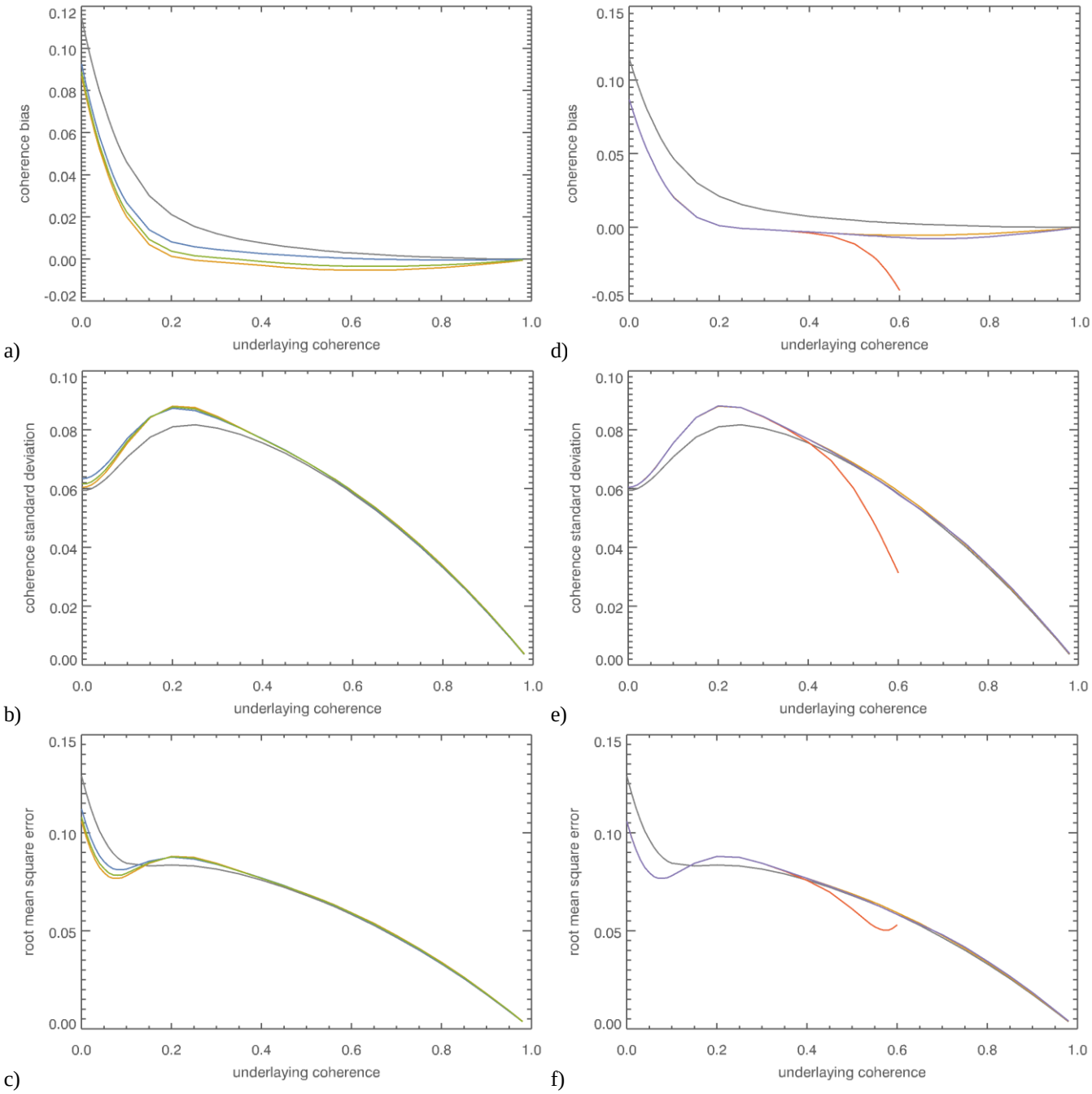

Fig. 15. Characteristic of estimators for 60 looks;
left column provides the uninformative prior and the right column the informative prior;
■ sample estimator, ■ MAP, ■ EAP, ■ MEDAP each with uninformative prior,
■ $EAPSP_{0.6}$, ■ $EAPLSP_{0.6}$ both have an informative prior
a) and d) Estimation bias γ_{bias}
b) and e) Standard deviation γ_{σ}
c) and f) Root mean square error γ_{rmse}

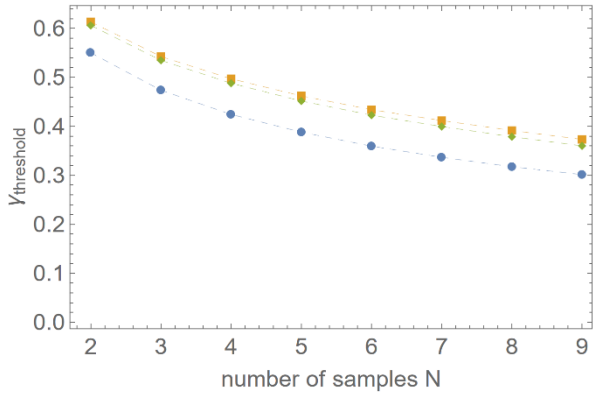

Fig. 16. Below each graph, the respective Bayesian estimator performs better than the sample estimator;
■ MAP, ■ EAP, ■ MEDAP each with uninformative prior.

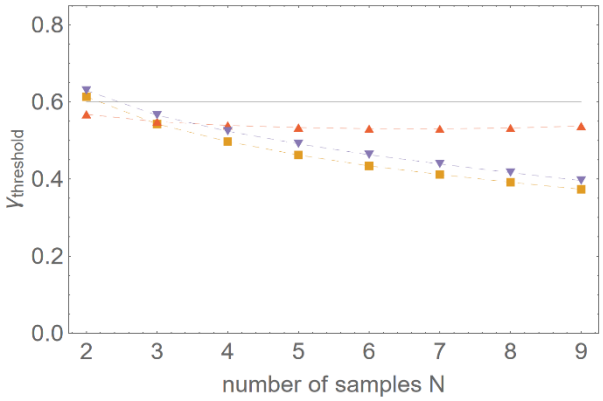

Fig. 17. Below each graph, the respective estimator performs better than the sample estimator, the grey line is the estimation range set by the general prior; ■ EAP, ■ $EAPLSP_{0.6}$, ■ $EAPSP_{0.6}$.

TABLE II

$\gamma_{threshold}$ FOR UNINFORMATIVE GENERAL PRIOR

N	2	3	4	5	6	7	8	9
EAP	0.61	0.54	0.50	0.46	0.44	0.41	0.39	0.37
MEDAP	0.61	0.54	0.49	0.45	0.42	0.40	0.38	0.36
MAP	0.55	0.48	0.42	0.39	0.36	0.34	0.32	0.30

TABLE III

$\gamma_{threshold}$ FOR INFORMATIVE GENERAL PRIOR

N	2	3	4	5	6	7	8	9
$EAPSP_{0.2}$	0.20	0.20	0.20	0.20	0.20	0.20	0.20	0.20
$EAPSP_{0.4}$	0.40	0.40	0.40	0.40	0.40	0.40	0.40	0.40
$EAPSP_{0.6}$	0.57	0.55	0.54	0.53	0.53	0.53	0.53	0.53
$EAPSP_{0.8}$	0.66	0.61	0.57	0.52	0.48	0.44	0.41	0.38
$EAPLSP_{0.2}$	0.59	0.53	0.49	0.46	0.43	0.42	0.40	0.38
$EAPLSP_{0.4}$	0.61	0.55	0.51	0.48	0.46	0.44	0.42	0.41
$EAPLSP_{0.6}$	0.63	0.57	0.52	0.49	0.46	0.44	0.42	0.40
$EAPLSP_{0.8}$	0.64	0.56	0.51	0.47	0.44	0.42	0.39	0.37

V. CONCLUSION

The principle of the empirical Bayes improves the coherence estimation from small samples and for small underlaying coherences and generally for a sample size $N \geq 15$ compared to the conventional sample estimator (4). The performance ranking results in the following order of the methods (best first): EAPSP, EAPLSP, EAP, MEDAP, MAP. Essentially, the more information is used and the stricter the general prior, the more accurate the estimate will be. For operational InSAR systems, it is recommended to implement the EAP method for straight forward coherence estimation without prior, the EAPLSP method for a known however less strict assumption on γ_{max} and the EAPSP method for the assumption that this value is always within the interval 0 - γ_{max}. The developed estimators are not limited to InSAR, but are generally applicable to coherence estimation problems from CCG processes.

VI. ACKNOWLEDGEMENT

I appreciate the work of the anonymous reviewers and I am grateful for the positive and very thorough comments and suggestions that helped improving the manuscript.

REFERENCES

[1] D. Derauw, "Phase unwrapping using coherence measurements," in *Proceeedings Synthetic Aperture Radar and Passive Microwave Sensing*, Paris, Nov. 1995.

[2] H. Zebker and J. Villasenor, "Decorrelation in interferometric radar echoes," *IEEE Transactions on Geoscience and Remote Sensing*, vol. 30, no. 5, pp. 950-959, Sept. 1992.

[3] D. Just and R. Bamler, "Phase statistics of interferograms with applications to synthetic aperture radar," *Applied Optics*, vol. 33, no. 20, pp. 4361-4368, Jul. 1994.

[4] P. Berardino, G. Fornaro, R. Lanari und E. Sansosti, „A new algorithm for surface deformation monitoring based on small baseline differential SAR interferograms," *IEEE Transactions on Geoscience and Remote Sensing*, Bd. 40, Nr. 11, pp. 2375-2383, Nov. 2002.

[5] A. Ferretti, A. Fumagalli, F. Novali, C. Prati, F. Rocca and A. Rucci, "A New Algorithm for Processing Interferometric Data-Stacks: SqueeSAR," *IEEE Transactions on Geoscience and Remote Sensing*, vol. 49, no. 9, pp. 3460-3470, Sept. 2011.

[6] G. Fornaro, S. Verde, D. Reale and A. Pauciullo, "CAESAR: An Approach Based on Covariance Matrix Decomposition to Improve Multibaseline–Multitemporal Interferometric SAR Processing," *IEEE Transactions on Geoscience and Remote Sensing*, vol. 53, no. 4, pp. 2050-2065, Apr. 2015.

[7] H. Ansari, F. De Zan und R. Bamler, „Sequential Estimator: Toward Efficient InSAR Time Series Analysis," *IEEE Transactions on Geoscience and Remote Sensing*, Bd. 55, Nr. 10, pp. 5637-5652, 10 2017.

[8] N. Cao, H. Lee and H. Jung, "Mathematical Framework for Phase-Triangulation Algorithms in Distributed-Scatterer Interferometry," *IEEE Geoscience and Remote Sensing Letters*, vol. 12, no. 9, pp. 1838-1842, Sept. 2015.

[9] R. Touzi and A. Lopes, "Statistics of the Stokes parameters and of the complex coherence parameters in one-look and multilook speckle fields," *IEEE Transactions on Geoscience and Remote Sensing*, vol. 34, no. 2, pp. 519-531, Mar 1996.

[10] R. Touzi, A. Lopes, J. Bruniquel and P. Vachon, "Coherence estimation for SAR imagery," *IEEE Transactions on Geoscience and Remote Sensing*, vol. 37, no. 1, pp. 135-149, 1999.

[11] H. Zebker and K. Chen, "Accurate estimation of correlation in InSAR observations," *IEEE Geoscience and Remote Sensing Letters*, vol. 2, no. 2, pp. 124-127, Apr. 2005.

[12] R. Abdelfattah and J.-M. Nicolas, "Interferometric SAR coherence magnitude estimation using second kind statistics," *IEEE Transactions on Geoscience and Remote Sensing*, vol. 44, no. 7, pp. 1942-1953, July 2006.

[13] M. Jiang, X. Ding and Z. Li, "Hybrid Approach for Unbiased Coherence Estimation for Multitemporal InSAR," *IEEE Transactions on Geoscience and Remote Sensing*, vol. 52, no. 5, pp. 2459-2473, May 2014.

[14] J. Goodman, "Some fundamental properties of speckle," *Journal of the Optical Society of America*, vol. 66, pp. 1145-1150, Nov 1976.

[15] J. O. Berger, Statistical decision theory and Bayesian analysis, New York: Springer, 1985, p. 617.

[16] J. Goodman, "Statistical Properties of Laser Speckle Patterns," in *Laser Speckle and Related Phenomena*, vol. 9, Berlin, Heidelberg, Springer, 1975.

[17] M. Seymour and I. Cumming, "Maximum likelihood estimation for SAR interferometry," in *Proceedings of IGARSS '94 - 1994 IEEE International Geoscience and Remote Sensing Symposium*, Pasadena, CA, USA, 1994.

[18] G. Carter, C. Knapp and A. Nuttall, "Statistics of the estimate of the magnitude-coherence function," *IEEE Transactions on Audio and Electroacoustics*, vol. 21, no. 4, pp. 388-389, Aug 1973.

[19] R. Bamler and P. Hartl, "Synthetic aperture radar interferometry," *Inverse Problems*, vol. 14, no. 4, pp. R1-R54, Feb. 1998.

Nico Adam received the Diploma degree in electrical engineering and telecommunication science from the University of Rostock, Germany in 1995. He has been with the German Aerospace Center (DLR), Oberpfaffenhofen, since 1995, where he manages SAR interferometry projects at DLR's Remote Sensing Technology Institute. His research interests include signal processing in the persistent scatterer interferometry framework, the use of numerical weather models to mitigate wave propagation effects in InSAR and the development of algorithms and software for advanced remote sensing radar systems. Relevant projects are the Shuttle Radar Topography Mission (DLR, NASA, ASI), TerraSAR-X (DLR), Terrafirma (ESA) and the Sentinel-1 Ground Motion Monitoring Service Germany. In 2017, he was honored as "DLR Senior Scientist" for his application-oriented work within projects.